Available online at www.sciencedirect.com

ScienceDirect

journal homepage: www.elsevier.com/locate/he

Kinetics study and modelling of steam methane reforming process over a NiO/Al_2O_3 catalyst in an adiabatic packed bed reactor

S.Z. Abbas[*], *V. Dupont*, *T. Mahmud*

School of Chemical and Process Engineering, The University of Leeds, LS2 9JT, UK

ARTICLE INFO

Article history:
Received 7 August 2016
Received in revised form
27 October 2016
Accepted 13 November 2016
Available online 9 December 2016

Keywords:
Mathematical modelling
Steam methane reforming
gPROMS MODELBUILDER 4.1.0®
Simulation
Diffusion limitation

ABSTRACT

Kinetic rate data for steam methane reforming (SMR) coupled with water gas shift (WGS) over an 18 wt. % NiO/α-Al_2O_3 catalyst are presented in the temperature range of 300–700 °C at 1 bar. The experiments were performed in a plug flow reactor under the conditions of diffusion limitations and away from the equilibrium conditions. The kinetic model was implemented in a one-dimensional heterogeneous mathematical model of catalytic packed bed reactor, developed on gPROMS model builder 4.1.0®. The mathematical model of SMR process was simulated, and the model was validated by comparing the results with the experimental values. The simulation results were in excellent agreement with the experimental results. The effect of various operating parameters such as temperature, pressure and steam to carbon ratio on fuel and water conversion (%), H_2 yield (wt. % of CH_4) and H_2 purity was modelled and compared with the equilibrium values.

Introduction

Increasing energy demand, depletion of fossil fuel reserves and pollution threats make hydrogen (H_2) an attractive alternative energy carrier. H_2 is widely considered as the fuel of the future due to its capability to drive the generation of electricity without emitting harmful pollutants [1]. More significantly, at present H_2 is the basic raw material for fertilizer industries especially for ammonia production as well as a necessary co-reactant for many refinery processes [2–5]. The oil refineries use a large quantity of H_2 in hydrocracking, hydrotreating, lubrication and isomerization processes [6]. With the passage of time it may become a general purpose carrier of energy for electricity, power generation and in vehicles as a transportation fuel [7–9]. When H_2 is burnt, the only product is water vapour, without greenhouse gas or any pollutant such as SO_x, soot and particular matters emitted in the environment [10–12].

Steam reforming of hydrocarbons, gasification of coal, enzymatic decomposition of sugar, conversion of glucose and alcohol are the few important processes of H_2 production [13]. At present, almost 90% of the worldwide H_2 originates from the fossil fuels [1]. Natural gas, naphtha and coal are the most common feedstocks for the production of H_2, but currently natural gas is the major source of H_2 production [14,15]. There are various options available for the production of H_2 by using natural gas as feedstock. Steam reforming, partial oxidation and auto-thermal reforming are the

* *Corresponding author.*
E-mail address: pmsza@leeds.ac.uk (S.Z. Abbas).
http://dx.doi.org/10.1016/j.ijhydene.2016.11.093

primary methods used for the production of H_2 by using hydrocarbons source [16].

Amongst all the available processes steam methane reforming (SMR) is the most established and commonly used process to produce syngas on a large scale [17]. Over 50% of the world's H_2 production comes from the SMR process [13]. The conventional SMR process used in industries consists of two main steps: in the first step endothermic SMR reaction (reaction (R1)) takes place at a high temperature (~800–1000 °C) and medium pressure (at 20–35 atm) and in the second step, the exothermic water gas shift (WGS) reaction (reaction (R2)) runs at a lower temperature (~200–400 °C) and medium pressure (10–15 atm) [18–20].

$$CH_{4(g)} + H_2O_{(g)} \leftrightarrow CO_{(g)} + 3H_{2(g)} \quad \Delta H_{298\ K} = +206\ kJ\ mol^{-1} \qquad (R1)$$

$$CO_{(g)} + H_2O_{(g)} \leftrightarrow CO_{2(g)} + H_{2(g)} \quad \Delta H_{298\ K} = -41\ kJ\ mol^{-1} \qquad (R2)$$

This two-step process of SMR enhances the H_2 production by shifting the reaction (R1) in the forward direction at a high temperature followed by reaction (R2) at a lower temperature. The overall SMR process is endothermic in nature and requires additional heat to proceed. The global SMR reaction is given as;

$$CH_{4(g)} + 2H_2O_{(g)} \leftrightarrow CO_{2(g)} + 4H_{2(g)} \quad \Delta H_{298\ K} = +165\ kJ\ mol^{-1} \qquad (R3)$$

The conventional steam methane reformer consists of a furnace that contains tubes in it, with catalyst loaded in these tubes to speed up the rate of the reaction (R1) [21].

The catalytic SMR is a complex process. It involves the diffusion of reactants through bulk of gases to the surface of the catalyst particles and within the porous particles as well. Many side reactions may take place as well. Considerable work has been done to generate the kinetics of SMR process by using different catalysts [22–26]. Many efforts have been made in the past to develop the most suitable catalyst for this process. There are many active metals used to promote the SMR process but nickel (Ni) is the most abundantly used metal because of its high reactivity and low attrition during set of experiments [27,28]. Ni is expensive as compared to few other available options, such as Mn, Fe and Cu, but this is compensated by using a lower percentage of Ni in the catalyst. Ni based catalyst can withstand very high temperature (900–1100 °C) and exhibits good mechanical strength. The use of alumina based supporting material has been investigated extensively in literature. It has been found that α-Al_2O_3 showed good reactivity and no agglomeration [29]. Depending upon the feed used, different metals and supports are used for steam reforming process [5,23,30–34].

The first kinetic study of the SMR was performed over Ni catalyst in the temperature range of 609–911 K [25]. In this kinetic study, the rate controlling step was the surface decomposition of methane. Later on, kinetics of SMR were derived on 12% Ni/Al_2O_3 at a slightly higher temperature range (823–953 K) [35].

Xu and Froment [22] presented the most widely used kinetic model for SMR. In their model they considered carbon dioxide (CO_2) as non-adsorbing gas on the surface of the catalyst. The reaction kinetics depend upon the partial pressure of the steam. According to Elnashaie et al. [35] partial pressure of steam has a negative effect on the reaction rate. Elnashaie et al. [35] presented different conclusions. According to their findings, partial pressure of steam has positive effect on the reaction kinetic. Xu and Froment's model includes both the positive and negative effect of the partial pressure of steam on the reaction kinetics, as it covered both the ranges of partial pressure of steam presented in the previous research. Later on, many authors demonstrated that Xu and Froment's model is more general than other models. Therefore, in this paper the kinetic model of Xu and Froment [22] will be used to describe the reaction kinetics.

Among the large numbers of reaction schemes, Xu et al. came up with a scheme, which considered all the reactions taking place during the SMR process [22]. This reaction scheme helped in formulating the rate of reactions of SMR process. The corresponding rate equations for reaction (R1)–(R3) are given in Appendix A.

The objective of this paper is to study the kinetics of the SMR process over 18 wt. % Ni/α-Al_2O_3 catalyst, and implement these kinetics in a 1-dimensional non-ideal plug flow heterogeneous model of the process in a laboratory-scale adiabatic packed bed reactor. Ni/α-Al_2O_3 catalyst is the most widely used catalyst in the industrial SMR process. The kinetic parameters (activation energy and pre-exponential coefficient) of the SMR process over 18 wt. % Ni/α-Al_2O_3 catalyst is not reported in the literature. In this study, the kinetic parameters of SMR process are developed and compared with the values reported by Xu and Froment [22] in their work by using Ni/$MgAl_2O_4$ catalyst. The 1-D heterogeneous model of SMR by using gPROMS model builder is also not reported in the literature. The developed kinetic parameters over Ni/α-Al_2O_3 catalyst are used in the gPROMS reactor model to study the process of SMR.

In this model only axial variation of process variables will be discussed. The choice of the catalyst was based on, according to our previous research, its ability to perform well under the cyclic redox conditions of chemical looping steam reforming [36,37], as well as in tandem with high temperature in-situ CO_2 capture by a solid sorbent, in a process called sorption enhanced steam reforming [38,39], using a wide range of organic feedstocks. The ultimate aim of obtaining the kinetic parameters for the SMR process with this particular catalyst in the present study is to build a realistic model of sorption enhanced chemical looping steam reforming of methane in packed bed configuration, and to be able to later adapt it to other, more sustainable organic feedstocks, with the aim of achieving sustainable and economical H_2 production with medium output, adaptable to remote sites using unconventional sources of feedstock.

Equipment and materials

The schematic diagram of the set-up used for the experimentation is shown in Fig. 1. This unit is divided into three sections relevant to feed, reformer reactor and analysis respectively. The feed section consists of gas cylinders for CH_4, N_2, H_2 and CO. MKS mass flow controllers were used to control the flow of gases going into the reactor. The N_2 mass

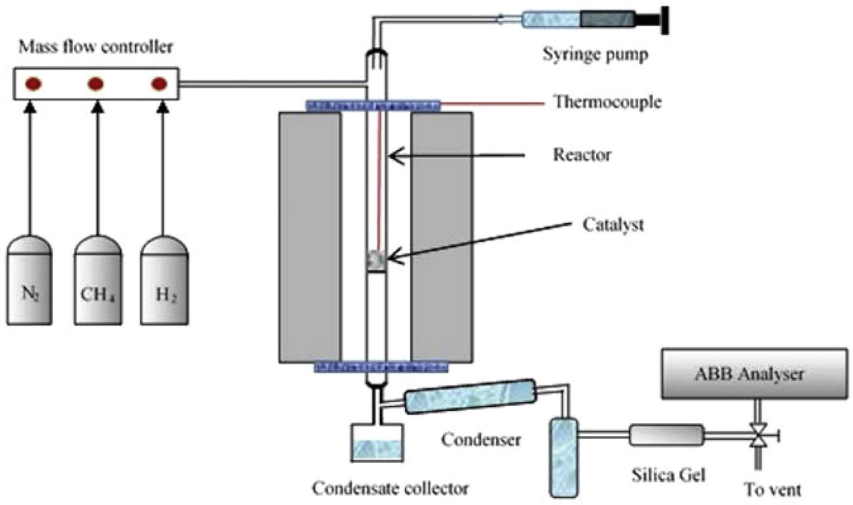

Fig. 1 – Experimental set-up for steam reforming process.

flow controller had the capacity of 10,000 cm^3/min (STP), CH_4 mass flow controller had 50 cm^3/min (STP) and H_2 mass flow controller had capacity of 500 cm^3/min (STP). Programmable syringe pump (New Era Pump Systems) was used to introduce a controlled amount of distilled water in the reactor to achieve a given molar steam to carbon (S/C) ratio in the reformer. The tubular reactor was made of quartz with an inner diameter of 1.2 cm and the length of 49.5 cm, held inside an electrically heated tube furnace (Elite Thermal Systems Ltd. TSV/12/50/300). The water entered into the top portion of the reformer where it evaporated and mixed with the controlled amount of gases. A known amount of catalyst (5.0 g) was placed in the middle part of the reactor. The catalyst used here is 18 wt. % NiO supported on α-Al_2O_3 provided by Johnson Matthey Plc. It was in the pellet form and was originally crushed to an average particle sizes of 1.2 mm, 1.85 mm, and 200 μm to determine the size resulting in the absence of pore diffusion limitation, with 200 μm used later in the kinetic study. The volume of the catalyst bed and bed length calculated was 2.67×10^{-6} m^3 and 0.030 m respectively. The particle density and thermal conductivity of solid is 1870 kg m^{-3} and 13.8 W m^{-1} K^{-1} respectively. The temperature inside the furnace was regulated by a Eurotherm 2416 temperature controller. The temperature of catalyst in the reactor, which may be slightly different from that of furnace (5–10 °C less), was monitored by a K-type thermocouple inserted at the centre of the catalyst bed. After the reaction, the product gases entered into the spiral tube condenser. The temperature of the condenser was set to −6 °C and ethylene glycol was used as the cooling agent in the chiller (Fisher Scientific 3016S). Water condensate was collected in the condensate collector. The analysers are very sensitive to water vapours; a silica gel trap was used to capture any water vapours leaving with product gases before entering into the analysers. The composition of outlet gases was analysed by Advanced Optima gas analyser from ABB and results were recorded online after every 5 s. The ABB analyser consisted of three analyser modules; Uras 14, Caldos 15 and Magnos 106. The Uras 14 was capable of detecting CH_4, CO_2 and CO based on infrared adsorption principle. The Caldos was used for H_2 measurement based on thermal conductivity. When required, the concentration of O_2 was measured by Magnos 106 analyser module. The uncertainties associated with the measurements were within ±3% on gas volume based.

The typical experimental run involved the following steps: **1)** Half an hour heating and purging of the reactor with N_2 gas. Temperature of the catalyst bed was raised to reaction temperature by using electrical furnace and simultaneously flushing the system with continuous flow of N_2 gas. **2)** After complete flushing of the system and ensuring that there was just N_2 present in the gas lines, N_2 flow was switched to the mixture of H_2 gas in N_2 (5 vol. % H_2 in N_2) for the reduction of the NiO catalyst, as the active phase of the catalyst is reduced Ni, whereas NiO is not catalytically active for steam reforming or water gas shift reactions. Reduction of the catalyst continued until the H_2 concentration returned to 5 vol. %, i.e. the initial concentration. **3)** Reduction was followed by flushing for an hour with N_2 gas to remove all the H_2 gas from the gas lines. **4)** The catalyst was then ready for SMR process. Before switching on the flow of fuel gas, water flow was started. Just after the introduction of water on the surface of catalyst, the flow of the fuel gas was switched on. This reaction process was allowed to run for a longer period of time (~4 h). Flow of the fuel gas and water was then turned off after obtaining steady state values of the concentration of all the exit gases. **5)** The system was again set on flushing and cooling.

Modelling methodology

Mathematical Modelling plays an important role in the development of a chemical reactor. It helps in understanding the experimentally observed processes by testing their reactor models on well-established software. A one-dimensional heterogeneous mathematical model with axial dispersion of the SMR process accounting for mass transfer in gas phase, mass transfer in solid phase, energy balance across the

reactor system and reaction kinetics was constructed. In this model it was assumed that,

a) Operation is adiabatic in nature
b) Ideal gas law is applicable
c) Concentration and temperature gradients along the radial direction are negligible. So, only one-dimensional variation in concentration and temperature i.e. in the axial direction is considered.
d) No temperature gradient is considered in the catalyst particles
e) Porosity of the bed is constant

To reduce the complexity in the modelling of the reaction kinetics, only those reactions which play a significant role in the overall process were considered. The chemical reactions used in the reactor modelling are (R1)–(R3) and their rate equations (A1)–(A3) are given in Appendix A. These rate expressions are based on Langmuir–Hinshelwood methodology as described and employed by Xu and Froment [22]. Mathematical model is composed of mass and energy balance equations both in the gas and solid phase. The mass, energy and momentum balance equations are given by:

Mass and Energy balance in the gas phase;

$$\varepsilon_b\left(\frac{\partial C_i}{\partial t}\right)+\frac{\partial(uC_i)}{\partial z}+k_{g,i}a_v(C_i-C_{i,s})=\varepsilon_b D_z\frac{\partial^2 C_i}{\partial z^2} \tag{1}$$

$$\varepsilon_b\rho_g C_{pg}\left(\frac{\partial T}{\partial t}\right)+u\rho_g C_{pg}\frac{\partial(T)}{\partial z}=h_f a_v(T_s-T)+\lambda_z^f\frac{\partial^2 T}{\partial z^2} \tag{2}$$

Mass and Energy balance in the solid phase;

$$k_{g,i}a_v(C_i-C_{i,s})+\left(\frac{\partial C_{i,s}}{\partial t}\right)=(1-\varepsilon_b)\rho_{cat}\,r_i \tag{3}$$

$$\rho_{bed}C_{p,bed}\left(\frac{\partial T_s}{\partial t}\right)+h_f a_v(T_s-T)=(1-\varepsilon_b)\rho_{cat}\sum -\Delta H_{rxn,j}\eta_j R_j \tag{4}$$

Pressure drop across the bed of reactor;

$$\frac{\Delta P g_c}{L}=\frac{150}{d_p^2}\left[\frac{(1-\varepsilon)^2}{\varepsilon^3}\right]\mu u+\left(\frac{1.75}{d_p}\right)\left(\frac{1-\varepsilon}{\varepsilon^3}\right)\rho_g u^2 \tag{5}$$

Boundary conditions;

At the reactor inlet (z = 0)

$$C_i=C_{i,0};\quad T=T_o;\quad T_s=T_{s,o};\quad P=P_o$$

At the reactor outlet (z = L)

$$\frac{\partial C_i}{\partial z}=0;\quad \frac{\partial T}{\partial z}=0;\quad \frac{\partial T_s}{\partial z}=0$$

Initial conditions;

$$C_i=C_{i,0};\quad T=T_o;\quad T_s=T_{s,o}$$

The rates of the SMR reactions are highly dependent upon the temperature of the system and concentration of the gases. The equilibrium constants and the kinetic rate constants in the rate equations [22] are given in Appendix A. The values for the pre-exponential factor and activation energy were obtained from the experiments performed in the laboratory (described in Section "Preliminary experiments"). The rate of formation or consumption of each component was obtained by combining reaction rate equations. The reaction rates for the species are given in Appendix A.

In mathematical modelling many physical properties are used like thermal conductivity, dispersion coefficient, mass transfer coefficient etc. The empirical correlations used to determine these properties are listed below.

Axial mass dispersion coefficient is given as [40];

$$D_z=0.73D_m+\frac{0.5ud_p}{1+9.49D_m/ud_p} \tag{6}$$

Effective thermal conductivity is given by the following relations [41];

$$\frac{\lambda_z^f}{\lambda_g}=\frac{\lambda_z^o}{\lambda_g}+0.75\mathrm{PrRe}_p \tag{7}$$

$$\frac{\lambda_z^o}{\lambda_g}=\varepsilon_b+\frac{1-\varepsilon_b}{0.139\varepsilon_b-0.0339+\frac{\left(\frac{2}{3}\right)\lambda_g}{\lambda_s}} \tag{8}$$

Mass transfer coefficient is given as [42];

$$k_{g,i}=j_{D,i}\mathrm{ReSc}_i^{1/3}\frac{D_i}{d_p} \tag{9}$$

$$\varepsilon_b j_{D,i}=0.765\mathrm{Re}^{-0.82}+0.365\mathrm{Sc}_i^{-0.398} \tag{10}$$

Dimensionless numbers are given as;

$$\mathrm{Re}=\frac{\rho_g u d_p}{\mu};\quad 0.01<Re<1500 \tag{11}$$

$$\mathrm{Sc}_i=\frac{\mu}{\rho_g D_i};\quad 0.6<\mathrm{Sc}<7000,\quad 0.25<\varepsilon_b<0.96 \tag{12}$$

Similarly, to determine the heat transfer coefficient and its dimensional numbers, following relations were used in the model formulation [42,43];

$$h_f=j_H\frac{C_{pg}G_s}{\mathrm{Pr}^{2/3}} \tag{13}$$

here,

$$j_H=0.91\mathrm{Re}^{-0.51}\psi;\quad 0.01<Re<50 \tag{14}$$

$$j_H=0.61\mathrm{Re}^{-0.41}\psi;\quad 50<Re<1000 \tag{15}$$

$$\mathrm{Pr}=\frac{C_{pg}\mu_g}{\lambda_g} \tag{16}$$

In the reactor model linear and non-linear partial differential equations (PDEs), algebraic equations, and initial and boundary conditions are involved, and gPROMS was used to solve these equations. The sensitivity of the model was first checked for discretization ranging from 10 to 1000 intervals and model was found independent of discretization. Finally, the laboratory reactor was axially discretized by 100 uniform intervals for this paper and output results were reported after every one second. The first order backward finite difference method (BFDM) of was used to solve the PDEs and algebraic equations using initial and boundary conditions as mentioned

above. The model of the adiabatic packed bed reactor was assumed to follow the non-ideal plug flow behaviour. In gPROMS differential algebraic solver (DASOLV) was used to solve the ordinary differential equation (ODEs). DASOLV converts the PDEs into ODEs, and 4th order Runge-Kutta technique was used to solve the system.

In order to compare the modelling results with an independent model, the chemical equilibrium and applications (CEA) software was used to generate the equilibrium data [44,45]. This software is based on minimization of Gibbs free energy (G) [46]; Equation (A15) in Appendix A. The thermodynamic analysis was done by considering the gas species involved in the reactant and product streams are CH_4, H_2, CO, CO_2, H_2O and N_2. The calculations were performed on the basis of N_2 balance. To study the effect of temperature, 1 bar and S/C of 3.0 was fixed. The thermodynamic calculations were allowed to run and outlet mole fraction data of product gases was collected for the calculations. Similarly to study the pressure effect, temperature and S/C conditions were fixed.

Preliminary experiments

Prior to the design of experiments for the derivation of kinetic rate parameters, preliminary experiments were performed to find out the size of the catalyst required to virtually eliminate the diffusion control limitations, a condition necessary to obtain true reaction kinetics. In general, the size of the particle is reduced to such a size where there are no diffusion effects. To this aim, the Weisz-Prater (WP) criterion was used to determine the required size of the particle [47,48], expressed as;

$$C_{WP} = \eta \emptyset_1^2 \tag{17}$$

With;

$$C_{WP} = \frac{-r'_A(obs)\rho_{cat}R_p^2}{D_e C_{A_s}} \tag{18}$$

If $C_{WP} << 1$, then there are no internal diffusion limitations and ultimately no concentration gradient exists within the catalyst particle. In order to find out how small the size of particle should be to avoid internal diffusion limitations, the Thiele Modulus ($\emptyset$) and the effectiveness factor (η) need to be calculated. The effectiveness factor is the measure of how far the reactant diffuses into the pellet before reacting. The Thiele modulus and the effectiveness factors are related to each other as follow:

$$\eta = \frac{3}{\emptyset_1^2}(\emptyset_1 \coth\emptyset_1 - 1) \tag{19}$$

$$\eta\emptyset_1^2 = 3(\emptyset_1 \coth\emptyset_1 - 1) \tag{20}$$

The reaction rate will be diffusion limited if the Thiele Modulus ($\emptyset$) is very large, i.e. if $\eta \ll 1$.

A first set of the experiments was performed by considering the size of particle (d_p) = 1.2 mm, to find out the size of the catalyst for which $\eta \cong 1$. Data for methane conversion (X_{CH_4}) was obtained and plotted against pseudo contact time defined by $W/F_{CH_4,o}$, to determine the rate of the reaction for this set of experiments. Weight (W) of the catalyst was kept constant in all of the experiments i.e. 5.0 g.

As expected, it was observed that as the flow rate of feed increased, keeping all the other parameters constant, conversion of CH_4 decreased due to the diminishing residence time. While keeping every parameter and operating conditions constant, except the size of the catalyst (d_p = 1.85 mm), for the second set of experiments, data for CH_4 conversion at different $W/F_{CH4,0}$ was obtained. As the size of the particle reduced, it increased the contact area and hence the conversion of CH_4 increased. Fig. 2 shows the effect of particle size and pseudo contact time on CH_4 conversion, and results were compared with equilibrium values as well.

The slope of both CH_4 conversion curves gives the rate of reaction of methane (r_{CH_4} in mol hr^{-1} $kgcat^{-1}$). Values for the Thiele modulus and the effectiveness factor for both sets of experiment were used to determine the size of the catalyst required for the kinetic study. As the size of catalyst reduced, the effectiveness factor approached unity. Calculated values for the Thiele modulus and effectiveness factor are shown in Table 1.

Table 1 shows that a particle size of 0.2 mm (200 μm) is required to virtually eliminate diffusion control (i.e. η = 0.92).

Results and discussion

Derivation of the kinetics of three SMR reactions

To ensure that the experiments were carried out in the region of intrinsic kinetics, the size of the catalyst particle was obtained in preliminary experiments. The experimental conditions used for the generation of kinetic parameters are listed in Table 2.

Typical curves of conversion of CH_4 against pseudo contact time are shown in Fig. 3 for a temperatures range between 550 °C and 700 °C. As expected for an endothermic process, increasing temperature and pseudo contact time has a

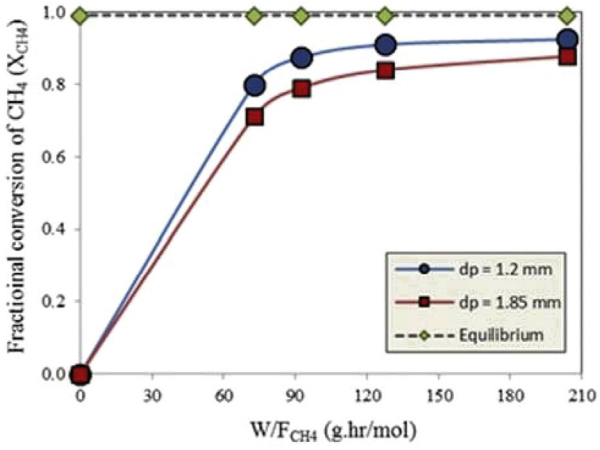

Fig. 2 – Effect of particle size and pseudo contact time on the conversion of CH_4 at constant S/C (3.12) and constant operating temperature (700 °C).

Table 1 – Calculated values for Thiele modulus and effectiveness factor.

Diameter of catalyst [mm]	Effectiveness factor	Thiele modulus
1.85	0.37	6.90
1.2	0.52	4.48
0.2	0.92	1.15

Table 2 – Experimental conditions.

Catalyst	18 wt. % NiO/α-Al_2O_3							
Diameter of catalyst, d_p [μm]	200							
Mass of catalyst [g]	5.0							
Reaction temperature [°C]	SMR				WGS			
	550	600	650	700	300	325	350	375
Pressure [atm]	1.0							
Molar S/C	3.12							
Feed mole fraction	CH_4		H_2O		N_2			
	0.075		0.234		0.691			
Feed volumetric flow rate at STP (cm^3/min)	CH_4		H_2O		N_2			
	10–28		0.023–0.064		92–258			

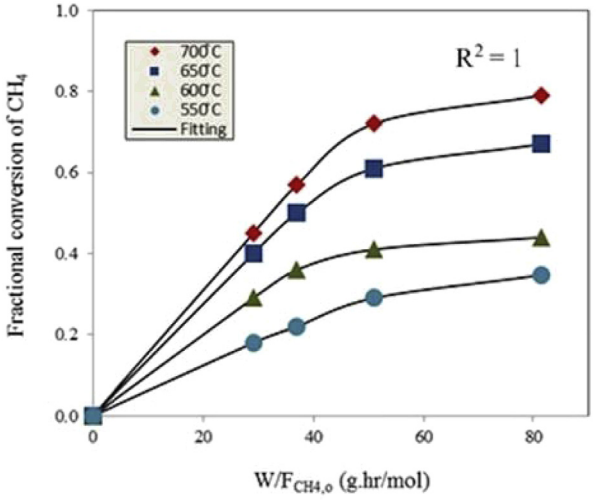

Fig. 3 – CH_4 conversion (X_{CH_4}) vs pseudo contact time ($W/F_{CH_4,o}$) for different temperature (550–700 °C), constant pressure (1 bar) and S/C of 3.12.

positive effect on the conversion of CH_4. Similarly, WGS reaction is very sensitive to temperature. Experiments were performed in the temperature range of 300–375 °C. Fig. 4 shows the variation of CO conversion with pseudo contact time at different temperature while keeping constant S/C of 3 and I bar pressure.

Third order polynomial regressions were used to correlate the conversion of CH_4 and conversion of CO with pseudo contact time. For a fixed temperature, pressure and molar S/C, the relationship between CH_4 and CO conversions with pseudo contact time is given as:

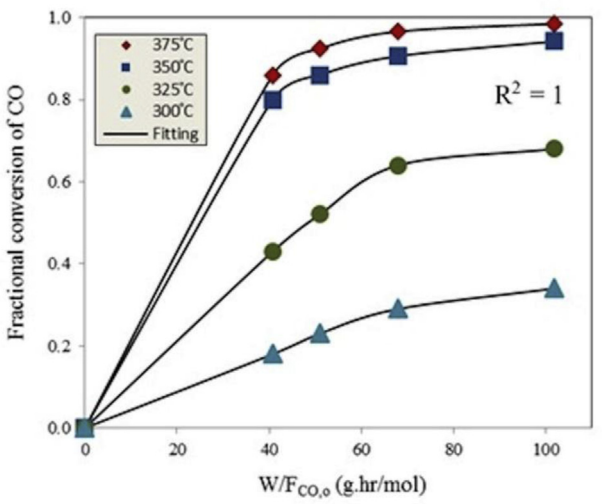

Fig. 4 – CO conversion (X_{CO}) vs pseudo contact time ($W/F_{CO,o}$) for different temperature (300–375 °C), constant pressure (1 bar) and S/C of 3.12.

$$X_{CH_4} = a_0 + a_1\left(\frac{W}{F_{CH_4}}\right) + a_2\left(\frac{W}{F_{CH_4}}\right)^2 + a_3\left(\frac{W}{F_{CH_4}}\right)^3 \quad (21)$$

$$X_{CO} = b_0 + b_1\left(\frac{W}{F_{CO}}\right) + b_2\left(\frac{W}{F_{CO}}\right)^2 + b_3\left(\frac{W}{F_{CO}}\right)^3 \quad (22)$$

CH_4 and CO disappearance rate can be obtained by differentiating Eqs. (21) and (22) w.r.t. (W/F_{CH_4}) *and* (W/F_{CO}). They are given as;

$$r_{CH_4} = \frac{dX_{CH_4}}{d\left(\frac{W}{F_{CH_4}}\right)} = a_1 + 2a_2\left(\frac{W}{F_{CH_4}}\right) + 3a_3\left(\frac{W}{F_{CH_4}}\right)^2 \quad (23)$$

$$r_{CO} = \frac{dX_{CO}}{d\left(\frac{W}{F_{CO}}\right)} = b_1 + 2b_2\left(\frac{W}{F_{CO}}\right) + 3b_3\left(\frac{W}{F_{CO}}\right)^2 \quad (24)$$

To estimate the kinetics parameters, a non-linear least square analysis based on minimization of the sum of the residual squares of the experimental reaction rates, obtained from Eqs. (23) and (24), and the predicted reaction rates, obtained from Eqs. (A10) and (A14), was employed. After successive iterations, the estimated values of the kinetic parameters were obtained. Figs. 3 and 4 show the good fitting of experimental data and regression data.

Temperature dependency of the reaction rate constants is shown in Fig. 5. The slope of the graphs in Fig. 5 gave the value of the activation energies, while the y-intercept provided the value of pre-exponential factors of the kinetic rate constant. The values for the activation energies and pre-exponential factors are listed in Table 3.

Model validation and sensitivity

In the following sections modelling results generated via gPROMS are presented and model is validated against the experimental results, performed in laboratory, and equilibrium outputs.

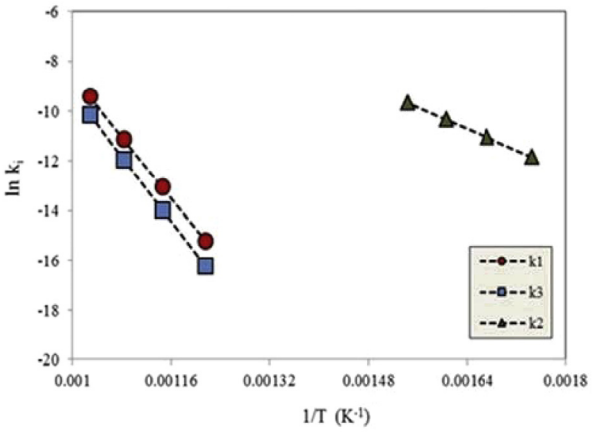

Fig. 5 – Temperature dependency of rate constants for reaction 1 (steam reforming), 2 (water gas shift) and 3 (combined steam reforming and water gas shift).

Dynamic behaviour of the packed bed reactor under conventional SMR

The dynamic transient profiles of molar concentration of CH_4, H_2, and CO_2 along the length of the reactor are shown in Fig. 6(a–c) for inlet temperature of 700 °C at S/C of 3. These results were generated with operating conditions tabulated in Table 4.

As the overall SMR reaction is endothermic in nature ($\Delta H_{298} = +165$ kJ mol^{-1}), therefore a drop in temperature of the reactor is expected during the conventional SMR process. In Fig. 6(a), dynamic profiles of temperature variation along the axial direction of the reactor under the operating conditions of 700 °C and 1 bar are presented between 0 and 400 s. The drop in temperature near the inlet of the reactor is about 50 K after 50 s and is the result of an overall endothermic reaction process. The temperature within the reactor reaches its steady state conditions after t ≥ 100 s. As the time increases, the drop in temperature along the length of the reactor also increases. When the reforming process is allowed to run for 400 s, a drop of 55 °C is observed at the end of the reactor. The variation of temperature with time causes variation of the molar concentration of the product gases. As expected, CH_4 concentration decreases along the axial direction of the reactor at all times during transient behaviour because of SMR reaction (R1) (Fig. 6(b)). The feed temperature (700 °C) is suitable for the reforming process. Hence, less amount of CH_4 is obtained at the outlet of the reactor as higher conversion of CH_4 is achieved at such a high temperature conditions. The concentration of CH_4 along the axial direction of the reactor increases with time. This can be explained by the variation of temperature along the axial direction of the reactor. The molar concentration of H_2 increases along the axial direction of the reactor (Fig. 6(c)). Similarly the amount of CO_2 is increasing along the axial direction of the reactor with the decrease in the amount of CH_4 (Fig. 6(d)). It can be seen that the response of molar concentration of these product gases is time dependent.

Table 3 – Activation energies and pre-exponential factors for SMR process via reactions 1 (SMR), 2 (WGS) and 3 (SMR/WGS) over 18 wt. % NiO/α-Al_2O_3.

Reaction parameters	This work	Xu and Froment [22]
E_1 [kJ mol^{-1}]	257.01	240.10
E_2 [kJ mol^{-1}]	89.23	67.13
E_3 [kJ mol^{-1}]	236.70	243.90
$k_{o,1}$ [mol bar$^{0.5}$ g^{-1} s^{-1}]	5.19×10^9	1.17×10^{12}
$k_{o,2}$ [mol bar^{-1}g^{-1}s^{-1}]	9.90×10^3	5.43×10^2
$k_{o,3}$ [mol bar$^{0.5}$ g^{-1} s^{-1}]	1.32×10^{10}	2.83×10^{11}

In an effort to study the kinetics of the SMR and WGS reactions, results are generated for rates of reactions (R1)–(R3). In Fig. 7(a–c) the variations of the reforming reaction rates at different locations of the reactor are presented. It can be seen that the SMR reaction (R1) is the dominant reaction at all locations within the reactor. At the very entrance of the reactor (z = 0.0012 m), the rate of SMR is maximum (Fig. 7(a)) and decreases drastically along the axial direction of the reactor (Fig. 7(b) and c). It can be explained by the temperature curve, as in the upstream zone of the reactor, the temperature of the system is maximum and it causes a large rate of SMR reaction (R1). The maximum rate of SMR in this zone of the reactor is 1.50 mol kg^{-1} s^{-1}. As the process is adiabatic in nature (q = 0) it causes the temperature of the system to drop from 700 °C (973.15 K) to 645.3 °C (918.15 K) along the length of the reactor. This drop in temperature results in the decrease in the rate of the endothermic reaction. As temperature at the entrance of the reactor is very high (~700 °C) and WGS shift reaction is not favourable at such a high temperature conditions. So, the rate of exothermic WGS shift reaction (R2) is very low in the upstream zone of the reactor and has a maximum value of 0.087 mol kg^{-1} s^{-1}.

As we move along the length of the reactor, the rate of reforming reaction decreases, caused by the drop in available CH_4 reactant. The maximum rate of SMR in the middle of reactor is ~0.0214 mol kg^{-1} s^{-1}. This is almost 70 times lower than the initial rate of the reforming reaction at the reactor entrance. It can be seen that as the rate of SMR reaction decreases, the conversion of CH_4 also reduces. In Fig. 7(b), it can be seen that the rate of WGS reaction is negative, indicating reverse reaction. This is because of temperature of the system, as higher temperature is not favourable for the WGS reaction.

At the end of the reactor, the rate of SMR reaction is even lower. The maximum value of SMR at the end of reactor is 0.011 mol kg^{-1} s^{-1} i.e. almost 136 times lower than the value obtained at the entrance of the reactor. It can be seen in Fig. 7(c) the rate of WGS reaction is higher than that at z = 0.0012 and 0.02 m. In Fig. 7(d), the steady state profiles of reforming reaction rate and temperature along the axial direction of the reactor are shown. The variation of temperature dictates the variation of the reforming reaction rates. It can be seen that high temperature at the entrance promotes the reforming reaction, but as the temperature of the system drops from 700 °C to 645 °C the SMR reaction rate also decreases. So the rate of SMR and global SMR reactions are maximum at the reactor entrance as can be seen in Fig. 7(d).

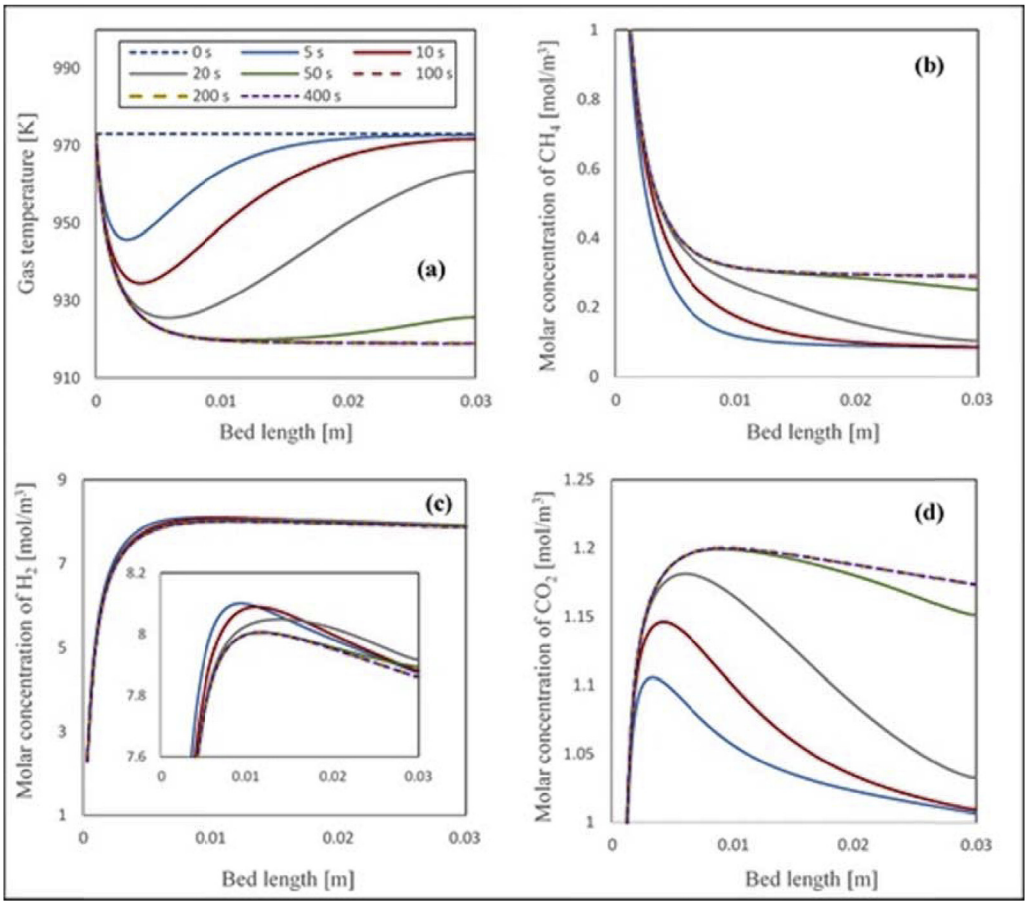

Fig. 6 – Dynamic profile of temperature profile and molar concentration of CH_4, H_2, and CO_2 in an adiabatic packed bed reactor at 700 °C, 1 bar, S/C of 3.0 and 0.05 kg m^{-2} s^{-1} mass flux of the gas phase conditions.

Model validation

The modelling results first need to be validated before further analysing the sensitivity of the SMR process. The model developed in gPROMS using the parameters and conditions listed in Table 4 was validated by comparing the modelling results with our experimental data. The t-value shows the percentage accuracy of the estimated parameters, with respect to 95% confidence interval. Model parameters satisfy the 95% confidence interval, and weighted residual had the value (7.32) less than that value of χ^2-value (100.75), which means the model was a good fit to the experimental values.

To validate the reactor model, two routes are adopted. In the first route, the modelling results are compared with their experimental counterparts far from the equilibrium conditions. Later on, the model is validated against the results generated, by using chemical equilibrium software, close to equilibrium conditions.

CASE 1: steady-state, away from equilibrium. In this section the experimental results generated under the steady-state conditions away from the equilibrium are compared with the equivalent modelling results. The modelling results need to satisfy both equilibrium and away from equilibrium conditions to be used as a flexible model. In the following section carbon balance results are used to validate the model.

a) Carbon balance and selectivity to carbon products

The rate equation for the carbon formation on the catalyst surface is not included in the developed model as the rate of formation of solid carbon is negligible as compared to the other rates. This is verified via the carbon

Table 4 – Operating conditions, parameters and average properties used in the reactor model.

Bed voidage [ε_b]	0.4
Bed length [L]	0.03 m
Density of catalyst [ρ_{cat}] [49]	1870 kg m^{-3}
Particle diameter [d_p]	1.2×10^{-3} m
Gas feed temperature [T]	700 °C
Catalyst temperature [T_s]	700 °C
Pressure [P]	1 bar
Bed heat capacity [$C_{p,bed}$] [15]	850 J kg^{-1} K^{-1}
Solid thermal conductivity [λ_s] [50]	13.8 W m^{-1} K^{-1}
Gas thermal conductivity [λ_g]	0.56 W m^{-1} K^{-1}
Molecular diffusivity [D_m]	1.6×10^{-5} m^2 s^{-1}
Steam to carbon ratio [S/C]	3.0

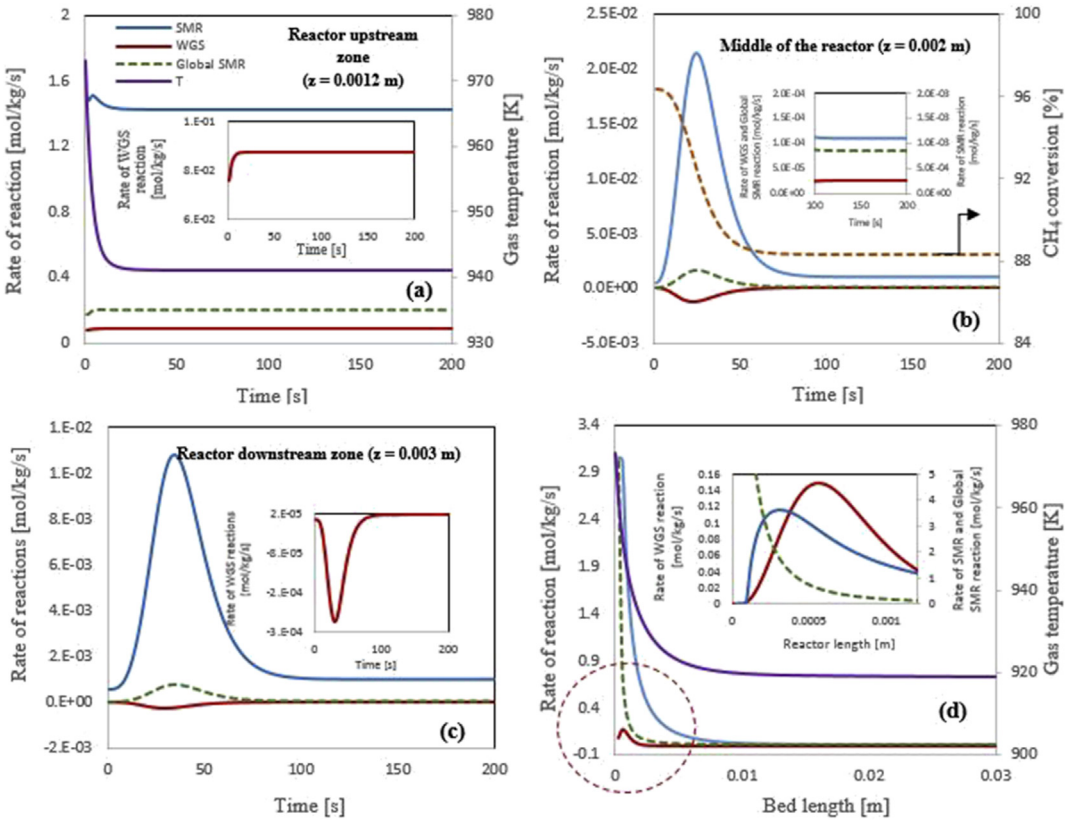

Fig. 7 – Model reaction rates at different location within an adiabatic packed bed reactor (a–c) and d) variation of reactions rate along the axial direction of reactor (under steady state conditions) at 700 °C, 1 bar, S/C of 3.0, 0.05 kg m^{-2} s^{-1} mass flux of the gas phase conditions.

balance across the reactor system for all the experiments performed for model validation and shown in Table 5. The maximum gas hourly space velocity (GHSV) used in the experimentation is 4.54 h^{-1} (equivalent to pseudo contact time of 73.1 g h mol^{-1}) and this caused 93% recovery of the feed carbon in the form of product gases CO, CO_2 and CH_4, while only 7% was unaccounted for which represents the largest percentage of carbon unaccounted for. This is most likely caused by the propagation of errors in each of the measured variables (feed rate of CH_4, and vol. % of CO, CO_2 and CH_4).

Selectivity (%) of CH_4 increased with increase in GHSV. As with the increase in GHSV, CH_4 conversion decreased and more CH_4 went in product gases. Mathematical model was developed by ignoring the kinetics of carbon formation rate, so according to modelling results all the carbon going in the feed is equal to the carbon going in the outlet gases. While on other hand, in experimental results, the amount of unaccounted carbon varied from 1.7 to 7%, depending upon the value of GHSV. In case of 1.62 h^{-1} GHSV, the amount of unaccounted carbon is almost negligible for both experiment and modelling and hence the selectivity of all the

Table 5 – Molar carbon balance for SMR experiments over 18 wt. % NiO/α-Al_2O_3 catalyst. Experiments were run over the duration of 4500 s, at 700 °C, 1 bar and S/C of 3.0.

GHSV (h^{-1}) [W/F in g h mol^{-1}]	Feed C (mol s^{-1})	C in outlet gases (mol s^{-1})			Exp. C out (mol s^{-1})	Exp. C_{out}/C in (%)
		CH_4	CO	CO_2		
1.62 [203.6]	0.030	E: 2.2×10^{-3} M: 1.8×10^{-3}	E: 1.38×10^{-2} M: 1.53×10^{-2}	E: 1.35×10^{-2} M: 1.38×10^{-2}	0.0295	98.30
2.58 [127.4]	0.049	E: 4.13×10^{-3} M: 5.1×10^{-3}	E: 2.00×10^{-2} M: 2.18×10^{-2}	E: 2.32×10^{-2} M: 2.18×10^{-2}	0.0472	96.33
4.54 [73.1]	0.086	E: 1.85×10^{-2} M: 1.77×10^{-2}	E: 2.55×10^{-2} M: 2.79×10^{-2}	E: 3.60×10^{-2} M: 3.39×10^{-2}	0.0800	93.02

Where E: Experimental data and M: Modelling data.

Table 6 – Comparison of experimental and modelling values of selectivity of C-based products at 700 °C, 1 bar and S/C of 3.0.

Gases	Experimental data [%]	Modelling data [%]
CH_4	7.6	5.4
CO	47	49.8
CO_2	45.5	44.8

carbon gases is quite comparable. The selectivity data for CH_4, CO and CO_2 under the operating conditions of 700 °C, 1 bar pressure and S/C of 3.0 in case of experiment and modelling is shown in Table 6.

Selectivity of hydrogen-containing products to H_2 obtained through experiments was in good agreement with the value obtained through the modelling work. For the range of GHSV (1.62–4.54 h^{-1}), H_2 selectivity in case of experiments varied from 92.6 to 97.7%. In case of modelling under the same operating conditions, it varied from 93.2 to 98.4%.

b) Conversion of CH_4 and H_2O

The comparisons of conversions obtained from experiments and predicted values are shown in Fig. 8(a–c). The experimental and predicted values for CH_4 and H_2O conversion are compared at 700 °C, 1 bar and S/C of 3.0. The predicted values are in good agreement with the values obtained from the experiments. To calculate the value of CH_4 conversion the following relation is used;

$$X_{CH_4} = \frac{(m_{CH_4,i} - m_{CH_4,o})}{m_{CH_4,i}} \times 100 \quad (25)$$

where m_{CH_4} represents the appropriate methane molar flows, with subscripts i and o standing for 'at reactor inlet and outlet' respectively. The selection of GHSV is very important here as achieving the equilibrium condition is not desirable. It can be seen that for each GHSV condition the reactor has successfully attained steady state and is closely reproduced by the model in the range of partial CH_4 conversions (0.79–0.93), i.e. far from the equilibrium. Under the same conditions, equilibrium would have yielded CH_4 and H_2O conversions of 99.9% and 47% respectively.

c) Hydrogen yield (wt. % of CH_4) and purity

Hydrogen yield (wt. % of CH_4) was calculated by using Eq. (26):

$$H_2 \text{ yield } (\text{wt. \% of } CH_4) = \frac{\left(\dot{n}_{H_2} \times \text{M.W of } H_2\right)}{\left(\dot{n}_{CH_4,in} \times \text{M.W of } CH_4\right)} \times 100 \quad (26)$$

where $\dot{n}_{H_2}$ and $\dot{n}_{CH_4,in}$ is the outlet molar flowrate of H_2 and inlet molar flowrate of CH_4 respectively.

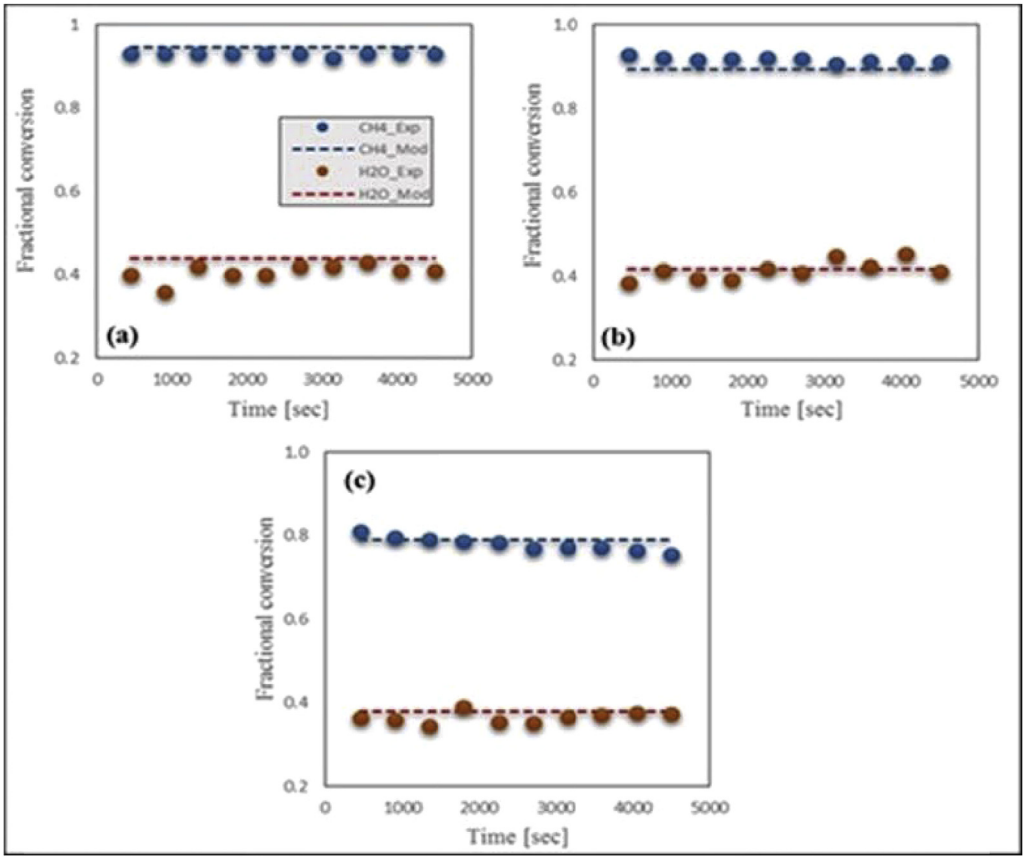

Fig. 8 – Comparison between measured and estimated CH_4 and H_2O conversion at 700 °C, 1 bar and S/C of 3. (a) 1.62 h^{-1} GHSV (b) 2.58 h^{-1} GSHV (c) 4.54 h^{-1} GHSV.

Fig. 9(a–c) shows the variation of H_2 purity and H_2 yield (wt. % of CH_4) with time. Modelling results are compared with the experimental results and a good agreement is observed.

Together with Table 5, Figs. 8 and 9 demonstrate the excellent agreement between experimental and predicted values and provided validation for the model based on three conditions away from the chemical equilibrium.

CASE 2: at equilibrium

Effect of temperature, S/C ratio and pressure on equilibrium. The model's outputs at equilibrium conditions were compared against those of the CEA model provide by NASA to further its validation. This was performed in the following conditions:

a) Effect of temperature

In the SMR process at equilibrium, temperature has a positive effect on purity and yield of H_2 up to peak values corresponding to complete CH_4 conversion by SMR followed by WGS. Beyond the temperature of peak yield, CH_4 conversion remains maximum but reverse WGS decreases steadily the H_2 yield and purity. Fig. 10(a) shows the effect of temperature on CH_4 and H_2O conversion at constant pressure (1.5 bar) and constant S/C (3).

b) Effect of pressure

Pressure is one of the important operating parameters in SMR process. The reforming process generates a larger amount of product moles (4) than the initial moles of reactant (3), thus, according to Le Chatelier's principle, low pressure favours the process, as it counteracts the rise in total molar concentration. On other hand, WGS reaction is equimolar and thus is not sensitive to pressure changes once equilibrium is reached. So the conversion of CH_4 at a fixed temperature goes down as the pressure of the system increases. Effect of pressure on conversion (CH_4 and H_2O), at constant temperature (600 °C) and constant S/C of 3, is presented in Fig. 10(b).

c) Effect of molar S/C

S/C plays a very important role in the overall performance of the system. Higher the S/C, higher will be the overall

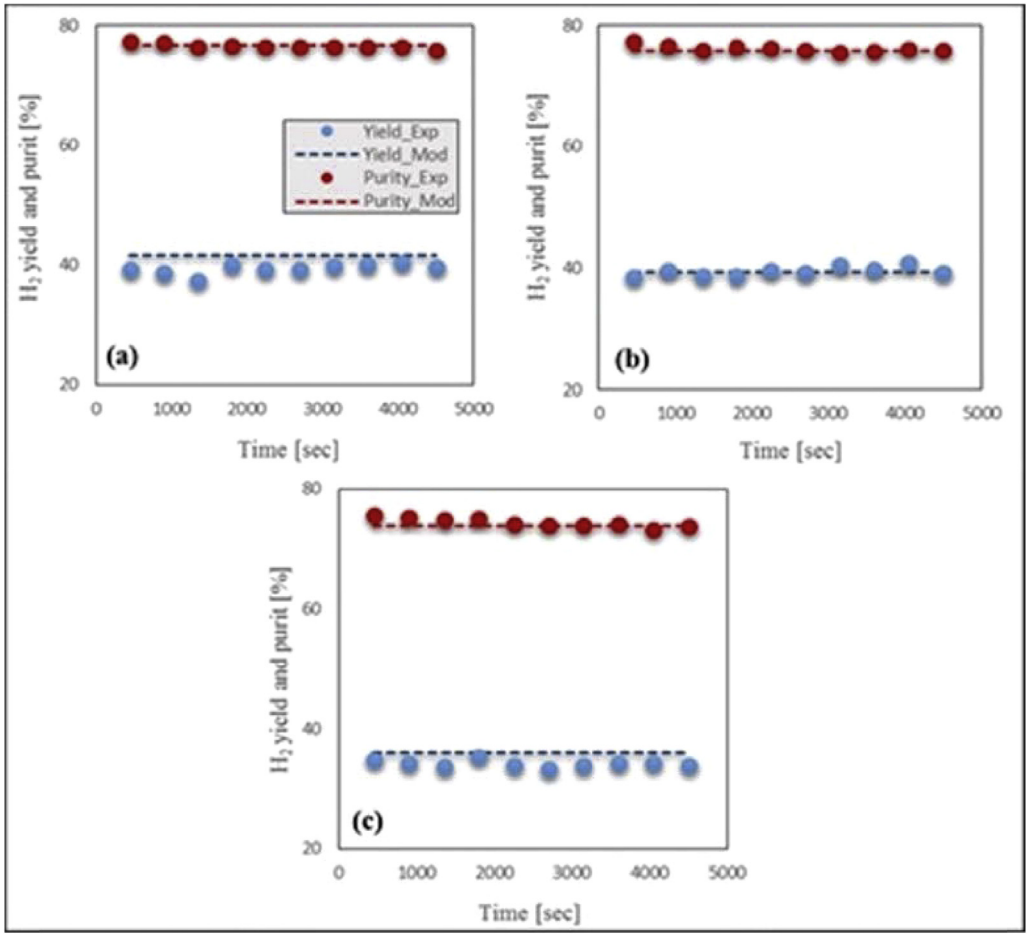

Fig. 9 – Comparison between measured and estimated values of H_2 purity (%) and H_2 yield (wt. % of CH_4) at 700 °C, 1 bar and S/C 3. (a) 1.62 h^{-1} GHSV (b) 2.58 h^{-1} GSHV (c) 4.54 h^{-1} GHSV.

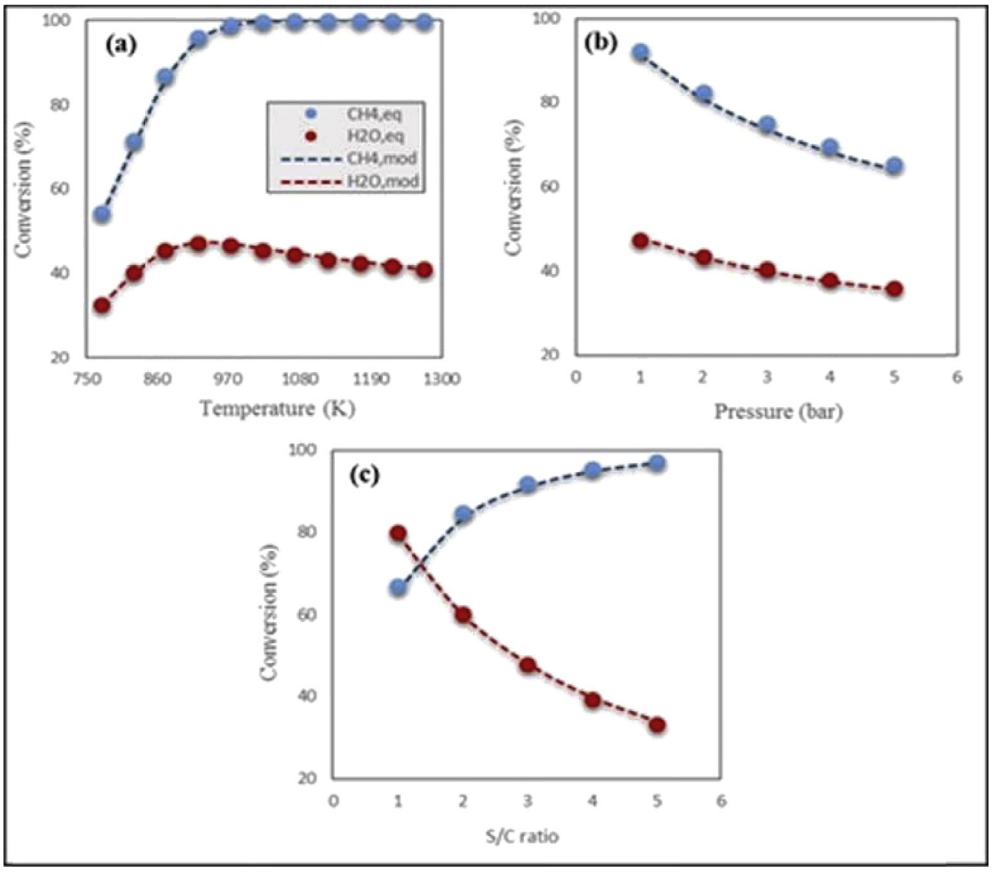

Fig. 10 – Effect on CH_4 and H_2O conversion of a) temperature, b) pressure and c) molar S/C.

conversion of the fuel (CH_4). But as the S/C increases, more energy is required to produce the required amount of steam and it affects the overall operational cost of the process. The Optimum S/C is the trade-off between the overall performance and cost of the process.

The effect of S/C on the conversion (CH_4 and H_2O), at constant temperature (600 °C) and constant pressure (1 bar), is presented in Fig. 10(c).

Model outputs away from equilibrium

Having demonstrated the validity of the model at and away from equilibrium, the model outputs are discussed in steady-state conditions away from equilibrium outside the range of our experimental data. Fig. 11 (a) shows the decrease of CH_4 and H_2O conversions for the increasing values of gas hourly space velocity (GHSV). The GHSV plays a vital role in the overall conversion of CH_4 and performance of the system. The higher the GHSV, i.e. the shorter the contact time with the catalyst throughout the reactor, the lower will be the CH_4 conversion. The modelling results were checked for different GHSV and results are presented in Fig. 11 (a–c). Selectivity to effluent gases was modelled according to the following equations;

$$H_2 \text{ selectivity } (\%) = \frac{n_{\dot{H}_2}}{\left(n_{\dot{CH}_4} + n_{\dot{H}_2}\right)} \times 100 \quad (27)$$

$$CH_4 \text{ selectivity } (\%) = \frac{n_{\dot{CH}_4}}{\left(n_{\dot{CH}_4} + n_{\dot{CO}_2} + n_{\dot{CO}}\right)} \times 100 \quad (28)$$

$$CO_2 \text{ selectivity } (\%) = \frac{n_{\dot{CO}_2}}{\left(n_{\dot{CH}_4} + n_{\dot{CO}_2} + n_{\dot{CO}}\right)} \times 100 \quad (29)$$

$$CO \text{ selectivity } (\%) = \frac{n_{\dot{CO}}}{\left(n_{\dot{CH}_4} + n_{\dot{CO}_2} + n_{\dot{CO}}\right)} \times 100 \quad (30)$$

where, $n_{\dot{H}_2}$, $n_{\dot{CH}_4}$, $n_{\dot{CO}_2}$, $n_{\dot{CO}}$ are the outlet molar flowrates of H_2, CH_4, CO_2 and CO respectively.

Thermal efficiency of reformer process is defined as;

$$\text{Thermal efficiency } (\%) = \frac{(\text{moles of } H_2 \text{ at outlet} \times LHV_{H_2})}{(\text{moles of } CH_4 \text{ in inlet} \times LHV_{CH_4})} \times 100 \quad (31)$$

where LHV is the relevant lower heating value.

Fig. 12 shows the variation of thermal efficiency of the reforming process with temperature at different S/C. The higher the S/C and temperature, the higher is the thermal efficiency of the process. Modelling results are compared with the equilibrium results, generated on CEA, and it was found that at temperature 750 °C and S/C of 3, equilibrium results for thermal efficiency are same as that of modelling results. At 700 °C and S/C of 3, thermal efficiency of the process is found to be 89.1%. GHSV used for Fig. 12 was 1.52 hr^{-1}.

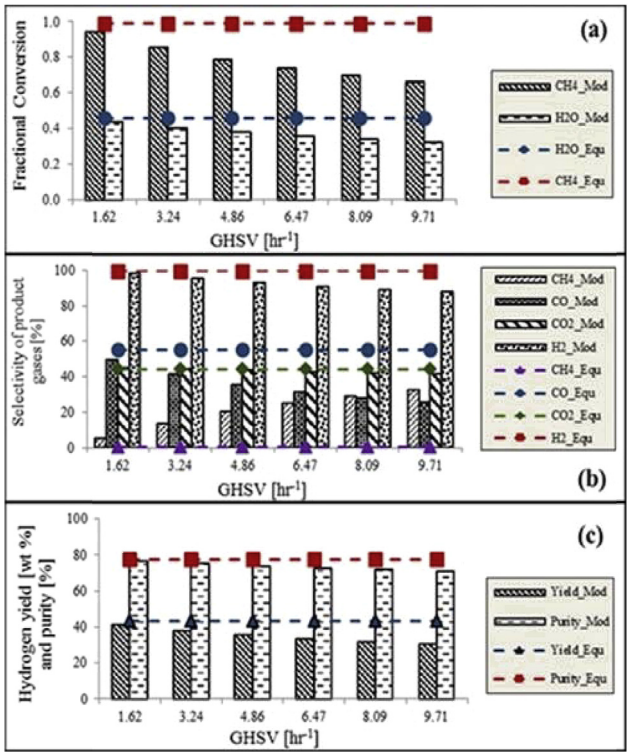

Fig. 11 – Effect of GHSV on a) conversion of CH_4 and H_2O, b) Selectivity to effluent gases (C-selectivity for CO, CH_4 and CO_2 and H-selectivity for H_2) & c) H_2 yield and purity, at 700 °C, 1 bar and S/C of 3.12.

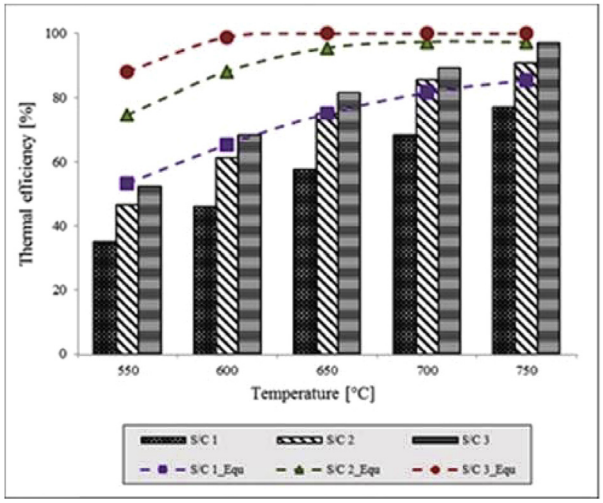

Fig. 12 – Effect of temperature and S/C on the thermal efficiency (%) of reforming process at 700 °C, 1 bar and 1.52 hr^{-1} GHSV.

Conclusion

An experimental study was performed over the surface of 18wt. % NiO/α-Al_2O_3 catalyst, to find out the reaction kinetics of the steam methane reforming process while keeping in mind the condition of diffusion limitations and far from the equilibrium conditions. The kinetic model proposed by Xu and Froment [22] is selected to fit the experimental data. A non-linear least square analysis based on minimization of the sum of the residual squares of the experimental reaction rates and the predicted reaction rates is used to estimate the kinetic parameters. The activation energies for SMR, WGS and global SMR reactions are calculated as 257.01 kJ mol^{-1}, 89.23 kJ mol^{-1} and 236.7 kJ mol^{-1} respectively.

The SMR process performance in terms of fuel conversion, selectivity of outlet gases, H_2 purity and yield (wt. % of CH_4 fed) is demonstrated in a fixed bed reformer using a 1-D heterogeneous reactor model. The modelling results are validated against the experimental results under the conditions of far from equilibrium. Later on, the modelling results are compared with the equilibrium results and an excellent agreement is observed. High temperature, lower pressure and high steam to carbon ratio gave the excellent performance of the system in terms of CH_4 conversion and purity of H_2. Results presented in this chapter gave the complete mathematical modelling of adiabatic fixed bed SMR reactor and this model will further be used for modelling sorption enhanced steam methane reforming (SE-SMR), chemical looping steam reforming (CL-SR) and sorption enhanced chemical steam reforming (SE-CLSR) processes for H_2 production.

Acknowledgement

The following are gratefully acknowledged: The financial support of University of Engineering and technology (UET) Lahore, Pakistan (Estab/D-412(327)/(2012)), Gaurav Nahar for help in the lab, Feng Cheng for help with CEA modelling and Jim Abbott at Johnson Matthey Plc (Billingham) for the NiO catalyst. We are also thankful for UKCCSRC EPSRC consortium (EP/K000446/1) call 2 grant 'Novel Materials and Reforming Process Route for the Production of Ready-Separated $CO_2/N_2/H_2$ from Natural Gas Feedstocks'.

Metadata for this paper can be found at http://doi.org/10.5518/126 in the form of an excel file.

Nomenclature

a_v	External surface area per unit volume of catalyst bed, $m^2\ m^{-3}$
C_i	Concentration of gases i, mol m^{-3}
$C_{i,o}$	Initial concentration of gases i in gas phase, mol m^{-3}
$C_{i,s}$	Concentration of gases i in solid phase, mol m^{-3}
$C_{s,o}$	Initial concentration of gases i in solid phase, mol m^{-3}
$C_{p,bed}$	Heat capacity of catalyst bed, J $(kg\ K)^{-1}$
C_{pg}	Heat capacity of gases, J $(kg\ K)^{-1}$
D_i	Effective diffusion coefficient, $m^2\ s^{-1}$
D_m	Average molecular diffusivity, $m^2\ s^{-1}$
D_z	Axial dispersion coefficient, $m^2\ s^{-1}$
d_p	Particle diameter, m
E_j	Activation energy of reaction j, J mol^{-1}
G	Gibbs free energy, J
G_s	Mass velocity of gases, kg $(m^2\ s)^{-1}$

ΔH_i	Heat of adsorption of i specie, J mol^{-1}
$H_{rxn,j}$	Heat of reaction of j reaction, J mol^{-1}
h_f	Gas to solid heat transfer coefficient, W $(m^2\ s)^{-1}$
j_D, j_H	Chilton-Colburn factor for mass and heat transfer
$k_{g,i}$	Gas to solid mass transfer coefficient of component i, $m^3\ (m^2\ s)^{-1}$
k_j	Kinetic rate constant of reaction j
k_{oj}	Reference temperature dependent kinetic rate constant of reaction j
K_j	Thermodynamic equilibrium constant
K_i	Adsorption constant of species i
K_{oi}	Reference adsorption constant of species i
K_D	Viscous loss term in pressure drop calculations, Pa s m^{-2}
K_v	Kinetic loss term in pressure drop calculations, Pa $s^2\ m^{-3}$
P_i	Partial pressure of species i, bar
P	Total gas pressure, bar
P_o	Initial pressure of the system, bar
Pr	Prandtl number
r_i	Rate of formation or consumption of species i, mol $(kg_{cat}\ s)^{-1}$
R_j	Rate of reaction j, mol $(kg_{cat}\ s)^{-1}$
R_g	Ideal gas constant, J $(mol\ K)^{-1}$
Re	Reynolds number
s	Active site of the catalyst
Sc_i	Schmidt number
T	Gas temperature, K
T_o	Gas inlet temperature, K
T_s	Catalyst temperature, K
$T_{s,o}$	Initial catalyst temperature, K
u	Superficial velocity of the gases, m s^{-1}
z	Axial dimension, m

Greek letters

Ω	Unit less term used in reaction kinetics
ε_b	Bed porosity
η_j	Effectiveness factor of reaction j
λ_g	Average gas thermal conductivity, W $(m\ K)^{-1}$
λ_s	solid thermal conductivity, W $(m\ K)^{-1}$
λ_z^f	Effective thermal conductivity, W $(m\ K)^{-1}$
μ_g	Average gas viscosity, kg $(m\ s)^{-1}$
μ_i	Chemical potential of component i, J mol^{-1}
ρ_{bed}	Bed density, kg m^{-3}
ρ_{cat}	Catalyst density, kg m^{-3}
ρ_f	Fluid density, kg m^{-3}
$\varnothing$	Thiele Modulus

Appendix A

$$R_1 = \frac{k_1}{p_{H_2}^{2.5}}\left(p_{CH_4}p_{H_2O} - \frac{p_{H_2}^3 p_{CO}}{K_I}\right)\left(\frac{1}{\Omega^2}\right) \quad (A1)$$

$$R_2 = \frac{k_3}{p_{H_2}}\left(p_{CO}p_{H_2O} - \frac{p_{H_2}p_{CO_2}}{K_{II}}\right)\left(\frac{1}{\Omega^2}\right) \quad (A2)$$

$$R_3 = \frac{k_2}{p_{H_2}^{3.5}}\left(p_{CH_4}p_{H_2O}^2 - \frac{p_{H_2}^4 p_{CO_2}}{K_{III}}\right)\left(\frac{1}{\Omega^2}\right) \quad (A3)$$

$$\Omega = 1 + K_{CO}p_{CO} + K_{H_2}p_{H_2} + K_{CH_4}p_{CH_4} + K_{H_2O}\frac{p_{H_2O}}{p_{H_2}} \quad (A4)$$

Equilibrium constants for steam methane reforming process, Arrhenius expression for kinetic parameters and adsorption equation are given as:

$$K_I = \exp\left(\frac{-26830}{T_s} + 30.114\right) \quad (A5)$$

$$K_{II} = \exp\left(\frac{4400}{T_s} - 4.036\right) \quad (A6)$$

$$K_{III} = K_I K_{II} \quad (A7)$$

$$k_j = k_{oj}\exp\left(\frac{-E_j}{R_g T}\right) \quad (A8)$$

$$K_i = K_{oi}\exp\left(\frac{-\Delta H_i}{R_g T}\right) \quad (A9)$$

Reaction rate for all species involved in the reactor system:

$$r_{CH_4} = -\eta_1 R_1 - \eta_3 R_3 \quad (A10)$$

$$r_{CO_2} = \eta_2 R_2 + \eta_3 R_3 \quad (A11)$$

$$r_{H_{2O}} = -\eta_1 R_1 - \eta_2 R_2 - 2\eta_3 R_3 \quad (A12)$$

$$r_{H_2} = 3\eta_1 R_1 + \eta_2 R_2 + 4\eta_3 R_3 \quad (A13)$$

$$r_{CO} = \eta_1 R_1 - \eta_2 R_2 \quad (A14)$$

Gibbs free energy:

$$dG = \sum_{i=1}^{N} \mu_i dn_i = 0 \quad (A15)$$

REFERENCES

[1] Chiron F-X, Patience GS, Rifflart S. Hydrogen production through chemical looping using NiO/$NiAl_2O_4$ as oxygen carrier. Chem Eng Sci 2011;66:6324–30.

[2] Harrison DP, Peng Z. Low-carbon monoxide hydrogen by sorption-enhanced reaction. Int J Chem React Eng 2003;1:1055.

[3] Ogden JM. Developing an infrastructure for hydrogen vehicles: a Southern California case study. Int J Hydrogen Energy 1999;24:709–30.

[4] Balasubramanian B, Lopez Ortiz A, Kaytakoglu S, Harrison D. Hydrogen from methane in a single-step process. Chem Eng Sci 1999;54:3543–52.

[5] Allen D, Gerhard E, Likins Jr M. Kinetics of the methane-steam reaction. Ind Eng Chem Process Des Dev 1975;14:256–9.

[6] Alves JJ, Towler GP. Analysis of refinery hydrogen distribution systems. Ind Eng Chem Res 2002;41:5759–69.

[7] Abrardo J, Khurana V. Hydrogen technologies to meet refiners' future needs: fuels management. Hydrocarb Process 1995;74:43–9.

[8] Liguras DK, Kondarides DI, Verykios XE. Production of hydrogen for fuel cells by steam reforming of ethanol over

supported noble metal catalysts. Appl Catal B Environ 2003;43:345–54.
[9] Winter C-J. Into the hydrogen energy economy—milestones. Int J Hydrogen Energy 2005;30:681–5.
[10] Rydén M, Ramos P. H_2 production with CO_2 capture by sorption enhanced chemical-looping reforming using NiO as oxygen carrier and CaO as CO_2 sorbent. Fuel Process Technol 2012;96:27–36.
[11] Ritter J, Ebner A. Separation technology R&D needs for hydrogen production in the chemical and petrochemical industries. US DOE Office of Industrial Technologies Program Report. 2005.
[12] Momirlan M, Veziroglu TN. The properties of hydrogen as fuel tomorrow in sustainable energy system for a cleaner planet. Int J Hydrogen Energy 2005;30:795–802.
[13] Cortright R, Davda R, Dumesic J. Hydrogen from catalytic reforming of biomass-derived hydrocarbons in liquid water. Nature 2002;418:964–7.
[14] Joensen F, Rostrup-Nielsen JR. Conversion of hydrocarbons and alcohols for fuel cells. J Power Sources 2002;105:195–201.
[15] Ding Y, Alpay E. Adsorption-enhanced steam–methane reforming. Chem Eng Sci 2000;55:3929–40.
[16] Ersoz A, Olgun H, Ozdogan S. Reforming options for hydrogen production from fossil fuels for PEM fuel cells. J Power Sources 2006;154:67–73.
[17] Rostrup-Nielsen JR, Sehested J, Nørskov JK. Hydrogen and synthesis gas by steam- and CO_2 reforming. Advances in Catalysis. Academic Press; 2002. p. 65–139.
[18] Adris A, Pruden B, Lim C, Grace J. On the reported attempts to radically improve the performance of the steam methane reforming reactor. Can J Chem Eng 1996;74:177–86.
[19] Fernández JR, Abanades JC, Murillo R, Grasa G. Conceptual design of a hydrogen production process from natural gas with CO_2 capture using a Ca–Cu chemical loop. Int J Greenh Gas Control 2012;6:126–41.
[20] Rosen M. Thermodynamic investigation of hydrogen production by steam-methane reforming. Int J Hydrogen Energy 1991;16:207–17.
[21] Kumar RV, Lyon RK, Cole JA. Unmixed reforming: a novel autothermal cyclic steam reforming process. Advances in Hydrogen Energy. Springer; 2002. p. 31–45.
[22] Xu J, Froment GF. Methane steam reforming, methanation and water-gas shift: I. intrinsic kinetics. AIChE J 1989;35:88–96.
[23] Hou K, Hughes R. The kinetics of methane steam reforming over a Ni/α-Al_2O catalyst. Chem Eng J 2001;82:311–28.
[24] Van Hook JP. Methane-steam reforming. Catal Rev Sci Eng 1980;21:1–51.
[25] Akers W, Camp D. Kinetics of the methane-steam reaction. AIChE J 1955;1:471–5.
[26] Berman A, Karn R, Epstein M. Kinetics of steam reforming of methane on Ru/Al_2O_3 catalyst promoted with Mn oxides. Appl Catal A General 2005;282:73–83.
[27] Rostrup-Nielsen JR. Catalytic steam reforming. Springer; 1984.
[28] Twigg MV, Twigg M. Catalyst handbook. CSIRO; 1989.
[29] Rydén M, Lyngfelt A, Mattisson T. Chemical-looping combustion and chemical-looping reforming in a circulating fluidized-bed reactor using Ni-based oxygen carriers. Energy & Fuels 2008;22:2585–97.
[30] Dirksen H, Riesz C. Equilibrium in the steam reforming of natural gas. Ind Eng Chem 1953;45:1562–5.
[31] Amphlett J, Evans M, Mann R, Weir R. Hydrogen production by the catalytic steam reforming of methanol: Part 2: kinetics of methanol decomposition using girdler G66B catalyst. Can J Chem Eng 1985;63:605–11.
[32] Cavallaro S, Freni S. Ethanol steam reforming in a molten carbonate fuel cell. A preliminary kinetic investigation. Int J Hydrogen Energy 1996;21:465–9.
[33] Wang D, Dewaele O, Froment GF. Methane adsorption on Rh/Al_2O_3. J Mol Catal A, Chem 1998;136:301–9.
[34] Peppley BA, Amphlett JC, Kearns LM, Mann RF. Methanol–steam reforming on Cu/ZnO/Al_2O_3. Part 1: the reaction network. Appl Catal A General 1999;179:21–9.
[35] Elnashaie S, Adris A, Al-Ubaid A, Soliman M. On the non-monotonic behaviour of methane—steam reforming kinetics. Chem Eng Sci 1990;45:491–501.
[36] Pimenidou P, Rickett G, Dupont V, Twigg M. Chemical looping reforming of waste cooking oil in packed bed reactor. Bioresour Technol 2010;101:6389–97.
[37] Dupont V, Ross A, Hanley I, Twigg M. Unmixed steam reforming of methane and sunflower oil: a single-reactor process for H_2-rich gas. Int J Hydrogen Energy 2007;32:67–79.
[38] Dou B, Rickett GL, Dupont V, Williams PT, Chen H, Ding Y, et al. Steam reforming of crude glycerol with in situ CO_2 sorption. Bioresour Technol 2010;101:2436–42.
[39] Dou B, Dupont V, Rickett G, Blakeman N, Williams PT, Chen H, et al. Hydrogen production by sorption-enhanced steam reforming of glycerol. Bioresour Technol 2009;100:3540–7.
[40] Edwards M, Richardson J. Gas dispersion in packed beds. Chem Eng Sci 1968;23:109–23.
[41] Yagi S, Kunii D, Wakao N. Studies on axial effective thermal conductivities in packed beds. AIChE J 1960;6:543–6.
[42] Geankoplis CJ. Transport processes and unit operations. 1993.
[43] Handley D, Heggs PJ. The effect of thermal conductivity of the packing material on transient heat transfer in a fixed bed. Int J Heat Mass Transf 1969;12:549–70.
[44] Gordon S, McBride BJ. Computer program for calculation of complex chemical equilibrium compositions and applications. Citeseer; 1996.
[45] McBride BJ, Gordon S. Computer program for calculation of complex chemical equilibrium compositions and applications II. Users manual and program description. 2; Users manual and program description. 1996.
[46] Kee RJ, Rupley FM, Miller JA. Chemkin-II: a Fortran chemical kinetics package for the analysis of gas-phase chemical kinetics. Livermore, CA (USA): Sandia National Labs.; 1989.
[47] Weisz P, Prater C. Interpretation of measurements in experimental catalysis. Adv Catal 1954;6:60390–9.
[48] Fogler HS. Elements of chemical reaction engineering. 1999.
[49] De Smet C, De Croon M, Berger R, Marin G, Schouten J. Design of adiabatic fixed-bed reactors for the partial oxidation of methane to synthesis gas. Application to production of methanol and hydrogen-for-fuel-cells. Chem Eng Sci 2001;56:4849–61.
[50] Halabi M, De Croon M, Van der Schaaf J, Cobden P, Schouten J. Modeling and analysis of autothermal reforming of methane to hydrogen in a fixed bed reformer. Chem Eng J 2008;137:568–78.